Characterization of the Vocal Fold Vertical Stiffness in a Canine Model

*Liran Oren, *Doug Dembinski, †Ephraim Gutmark, and *Sid Khosla, *†Cincinnati, Ohio

Summary: Objectives/Hypothesis. Characterizing the vertical stiffness gradient that exists between the superior and inferior aspects of the medial surface of the vocal fold. Characterization of this stiffness gradient could elucidate the mechanism behind the divergent glottal shape observed during closing.

Study Design. Basic science.

Methods. Indentation testing of the folds was done in a canine model. Stress-strain curves are generated using a customized load-cell and the differential Young's modulus is calculated as a function of strain.

Results. Results from 11 larynges show that stress increases as a function of strain more rapidly in the inferior aspect of the fold. The calculations for local Young's modulus show that at high strain values, a stiffness gradient is formed between the superior and inferior aspects of the fold.

Conclusions. For small strain values, which are observed at low subglottal pressures, the stiffness of the tissue is similar in both the superior and inferior aspects of the vocal fold. Consequently, the lateral force that is applied by the glottal flow at both aspects results in almost identical displacements, yielding no divergence angle. Conversely, at higher strain values, which are measured in high subglottal pressure, the inferior aspect of the vocal fold is much stiffer than the superior edge; thus, any lateral force that is applied at both aspects will result in a much greater displacement of the superior edge, yielding a large divergence angle. The increased stiffness observed at the inferior edge could be due to the proximity of the conus elasticus.

INTRODUCTION

During vocal fold vibration, the glottis can take a convergent shape during opening (where the inferior aspect between the vocal folds is wider than the superior aspect) and a divergent shape during closing. This convergent-divergent transformation stems from the mucosal wave traveling in the inferior-superior direction, which was noted qualitatively using a full larynx model (Hirano[1]) and detailed in a hemilarynx model (Jiang and Titze[2]). In both models, the authors noted that during opening, when viewed from above, the inferior aspect of the folds was hidden by the superior aspect, which suggested that the glottis assumed a converging shape. Jiang and Titze were able to visualize the glottal dynamics from a coronal view, noting that during closing, the medial displacement of the inferior aspect of the fold preceded the displacement of the superior aspect, implying that the glottis assumes a diverging shape during closing. According to the myoelastic-aerodynamic theory, the convergent-divergent shape of the glottis is formed due to a phase delay in the inferior-superior direction of the mucosal wave velocity (Titze and Alipour[3]).

The convergent-divergent shape transformation of the glottis also affects the dynamics of the intraglottal flow. The intraglottal flow will attach (ie, follow the contour) to the converging walls of the glottis during opening but will separate (ie, not follow the contour) from the diverging walls during closing. The intraglottal flow separation during closing was demonstrated in computational, mechanical, and excised canine models (Shadle et al,[4] Pelorson,[5] Alipour and Titze,[6] Zhao et al,[7] and Kucinschi et al[8]), but the influence of intraglottal flow separation, if any, on the vibrations of the vocal folds is still being evaluated.

It is well known in the field of fluid mechanics that flow separation can significantly alter the pressure distribution in the flow (Anderson[9]). During phonation, the intraglottal pressure distribution determines the forces applied on the glottal wall by the intraglottal flow. The impact of the forces generated by flow separation in the glottis varies according to the models being used: The two-mass model of Ishizaka and Flanagan[10] did not consider flow separation to occur during closing, whereas the three-mass model of Story and Titze[11] and Pelorson et al[5] accounted for flow separation in the glottis during closing, but for simplification assumed that the intraglottal pressure downstream of the separation point was atmospheric. Other computational models (Zhao et al,[7] Zhang et al,[12] and Mihaescu et al[13]) predicted that intraglottal flow separation could lead to intraglottal vortices forming near the superior aspect of the folds. These flow separation vortices can produce pressure that is less than atmospheric (ie, negative pressure), thus applying an additional suction force on the superior aspect of the folds during closing. The magnitude of the negative pressure that can develop near the superior aspect of the fold is determined by the dynamic characteristics of the flow, which are influenced by the magnitude of the divergence angle of the folds (Figure 1).

Because the divergence angle may affect intraglottal pressures, it is important to understand mechanisms that create and increase the divergence angle. Our work, using particle image velocimetry to determine intraglottal geometry and velocity fields (Oren et al[14]), shows that at low subglottal pressure (ie,

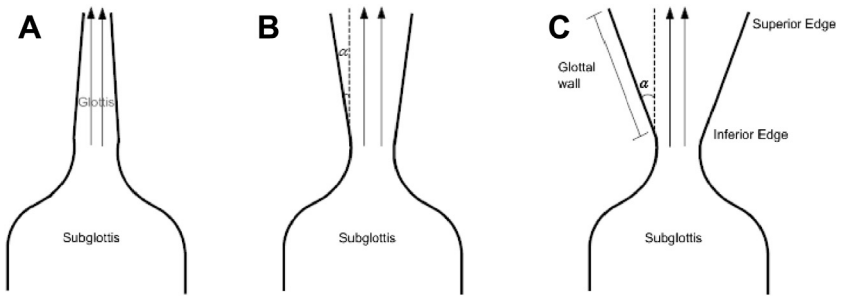

FIGURE 1. Schematics of the vocal folds vibration. (**A**) During opening, showing a convergent shape of the glottis. The intraglottal flow follows the contour of the wall. (**B**) During closing with a small divergence angle (α). The intraglottal flow may separate from the wall (**C**) during closing with a larger divergence angle. The intraglottal flow separates from the wall. Flow separation vortices may form in the glottis.

lung pressure), the divergence angle is small, and as the subglottal pressure increases, the divergence angle increases. The divergence angle will be increased by any factor that increases the phase difference between the upper and lower masses. It has been proposed in theoretical models that vocal tract inertance will increase this phase difference (Titze[15]). On the other hand, simulations done without a vocal tract show minimal phase difference (Story[16]). Our hypothesis for this behavior, and motivation for this study is that at low pressures, there is similar stiffness between the superior and inferior aspects of the fold; however, as subglottal pressure increases, the inferior aspect of the fold becomes stiffer than the superior aspect. This hypothesis attempts to address the question of how a phase delay can occur without a vocal tract.

The difficulty in accurate characterization of the elastic properties of the vocal folds stems from the inhomogeneous composition and viscoelastic characteristics of the tissue. The composition of the vocal fold tissue is often approximated by the two-layer body-cover model (Hirano[17]): The body, consisting of the deep layer of the lamina propria and the thyroarytenoid (TA) (vocalis) muscle, is largely responsible for maintaining muscular tone and accounts for the majority of the overall stiffness of the tissue (Titze and Alipour[3]). The cover, consisting of the epithelium and the superficial and intermediate layers of the lamina propria, is the locale most associated with mucosal wave propagation and has little mechanical integrity. The inhomogeneity of the body-cover layers also leads to an anisotropic response of the tissue.

The elastic properties of the vocal folds are most commonly studied in human or canine models. Canine vocal fold tissue is the preferred (animal) model because of the anatomical and acoustical similarities with human samples (Titze[18]). Additionally, testing in canines is performed immediately postmortem with minimal (or no) tissue decomposition, which reduces the variations in tissue properties that can stem from the decay process.

The data reported in the literature for the elastic properties of the vocal folds varies significantly depending on the specimen type and the testing method examined in the study (eg, the direction of loading). For example, Chan et al[19] used elongation technique to evaluate the longitudinal elastic properties of the tissue and showed that human males had higher levels of collagen in the tissue, which yielded a much higher Young's modulus (ie, stiffness) compared with females. Chan et al noted that the value for Young's modulus was a function of the strain in the tissue. At 40% strain level, they reported values of 1750/350 kPa for the ligament layer in human male/female, respectively, and 1000/480 kPa for the cover layer in male/female, respectively. These data can be compared with the data reported by Min et al[20] who used the same (elongation) technique but reported values of 600 kPa for the same (40%) strain level in the human ligament. Min et al did not show a gender-based difference like Chan et al, but their study was conducted on a smaller set of data (two males and two females compared with 12 males and eight females). Another study by Perlman and Durham[21] using human vocal fold tissue reported a longitudinal value of 400 kPa for the Young's modulus at 50% strain.

In the elongation technique, the vocal fold is normally mounted to the testing apparatus at its anterior/posterior ends and subject to a controlled tension. A drawback of this method is that it requires removal of the vocal fold from the larynx, eliminating the physiological prestress that is imparted on the fold by the surrounding tissue. The elongation technique then extracts the *global* longitudinal elastic properties. In comparison, the microindentation technique uses a solid indenter, which displaces the tissue a known distance and the resultant force is recorded. The microindentation technique neglects (local) tissue inhomogeneity that may exist in the tissue and allows for *local* elasticity variations to be resolved. The microindentation technique also allows the vocal fold to be kept intact in its normal physiological surroundings.

The microindentation technique was used by Chhteri et al[22] to evaluate the local elastic properties of human vocal folds at the mid-membranous plane. They noted that the stiffness of the tissue changes if the folds are removed from the larynx because of the elimination of the prestress condition. Chhetri et al showed that the inferior medial surface was stiffer than the superior medial surface. For a low strain value (vocal fold at rest), they measured a Young's modulus of 8.6 kPa at the mid-membranous plane. These data can be compared with the Young's modulus values reported by Berke and Smith[23] of 2.4 kPa (at low strain) and by Tran et al[24] who reported 7.6 kPa. Both these studies used microindentation at the mid-membranous plane.

Another measurement technique used to evaluate the elastic properties of the vocal folds is linear skin rheometry. The

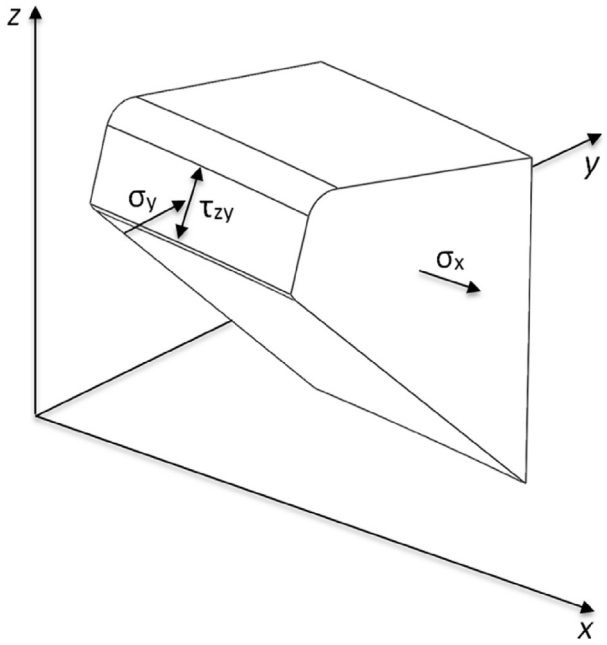

FIGURE 2. Schematic of the stress components that occur during the closing phase of vocal folds vibration. σ_x is the axial stress due to longitudinal tension (elongation of the folds). σ_y is the transverse stress due to the glottal flow and the lateral fold displacement. τ_{zy} is the transverse shear due to the glottal airflow.

technique is based on attaching a suction probe to the tissue and extracting the shear elastic properties. Goodyer et al[25] was able to measure the cover layer stiffness of the vocal fold at different planes in both the superior-inferior and anterior-posterior directions. They noted increased stiffness as a function of strain in the inferior and posterior direction in both canine and human larynges.

ELASTICITY PARAMETERS

The internal forces that develop in a deformed body are measured by stress, σ, which is defined as the ratio of force per area. Stress is a vector quantity and the term *normal stress* is used when the force is perpendicular to the area, whereas *shear stress* is used when the force is parallel to the area. *Cauchy stress* is the quantity that combines both normal and shear stresses: $\sigma = \overrightarrow{F}/A$. Figure 2 shows a schematic of the different stress components that develop during the closing phase of the folds. The glottal airflow and the lateral displacement of the folds produce normal (transverse) stress, σ_y. The glottal airflow also produces shear stress on the folds, τ_{zy}. The longitudinal tension, which determines the pitch, produces normal axial stress, σ_x.

The deformation of any point in a continuum space depends on the deformation that occurs in its proximity. This mode is often measured by strain, ε, which is defined as the ratio of the initial dimensions of the object to the dimensions of the object after a force is applied. Strain can stem from compression, tension, or both forces. The common *engineering strain* is measured (for a uniaxial compressive force) as: $\varepsilon = (L_0 - L)/L_0$, where L_0 is the initial length and L is the compressed (final) length. For tension strain, the initial length is subtracted from the final length. Engineering strain is commonly used when material deformation is small and the deformation gradients (between adjacent points) are negligible. Finite deformation, such as that observed in soft tissue, indicates that strain is large and, consequently, deformation gradients cannot be neglected. Instead of engineering strain, Fung[26] suggested using *Green's strain*, a quantity that is derived to account for the (large) deformation gradients, to characterize soft tissue. For a uniaxial compressive force, Green's strain is defined as:$\varepsilon_G = (L_0^2 - L^2)/2L_0^2$. Note that for a very small deformation $\varepsilon_G \approx \varepsilon$.

Young's modulus, E, is the conventional parameter used to evaluate material stiffness. In its simple form, Young's modulus denotes the ratio of the stress to strain: $E = \sigma/\varepsilon$. Calculating E in the familiar way assumes that the deformation of the material is linear, which is not a correct axiom when dealing with soft tissue elasticity. Previous studies used various nonlinear models to fit their elasticity data and compute the Young's modulus (Table 1) of the tissue.

Using the microindentation technique, this study aims to characterize the difference in the vertical stiffness that exists between the superior and inferior aspects of the medial surface of the fold. Stress-strain curves are generated in both the superior and inferior aspect of the folds and the Young's modulus of the tissue in both locations is calculated as a function of strain. Characterization of this stiffness gradient could further elucidate the mechanism behind the divergent glottal shape observed during closing. Viscoelastic properties of the tissue, such as creep and stress relaxation, were not considered in the present study.

METHOD

Eleven excised larynges (L1–L11) were harvested from shared research mongrel canines (mean weight 18.9 ± 1.8 kg) immediately after the animals were euthanized. The mean length of the membranous folds (defined from the vocal process to the anterior commissure) was 14.3 mm (±1.0 mm) and the mean vertical height (defined from the superior-medial edge to the inferior medial edge) was 2.5 mm (±0.5 mm). Testing was done 3–24 hours postmortem, and the larynges were kept in saline between experiments.

Force measurements were taken using a customized load cell (Sensing Systems, Inc., New Bedford, MA) with a full Wheatstone bridge configuration of strain gages bonded to the sensing element. The Wheatstone bridge provides a very sensitive electrical output signal as force is applied to the load cell. The load cell consisted of an arm (where the strain gages were attached) connected to a circular contact tip (1 mm diameter, 2 mm long) and was set to measure a 0–100 mN force range. A schematic of the load cell is shown in Figure 3A. The accuracy of the force measurements was within 0.3% of its full scale.

The larynx was mounted using a four-pronged support apparatus that was fixed to the cricoid. The folds were initially adducted together by placing a suture through both vocal processes at the same level. Adduction of the folds was necessary

TABLE 1.
Summary of Literature Data for Young's Modulus of Vocal Fold Tissue

Study	Species and Quantity	Measurement Method	Formula for E	E Value
Chhetri et al[22]	Human, 3	Microindentation	$E = (1 - \nu^2)/(2R) \times (dF/dh)$	Superior: 2.9 kPa Medial cover: 4.8 kPa Inferior: 7.5 kPa Body: 2.0 kPa
Chan et al[19]	Human, 20 (12 males, 8 females)	Longitudinal elongation	Linear portion: $\varepsilon = \Delta L/L_0$; $\sigma = a\varepsilon + b$; $E = d\sigma/d\varepsilon$ Nonlinear portion: $\varepsilon = Fp\,(L_0 + \Delta L)/m$; $\sigma = A\varepsilon e^{B\varepsilon}$; $E = d\sigma/d\varepsilon$	10% strain: 40 kPa 30% strain: 420 kPa (male), 185 kPa (female) 40% strain: 1750 kPa ligament (male), 1000 kPa cover (male), 350 kPa ligament (female), 480 kPa cover (female)
Min et al[20]	Human, 4	Longitudinal elongation	$\varepsilon = 100 \times (L_0 - L)/L$; $\sigma = F/A$; $E = \sigma/\varepsilon$	Low strain: 33.1 ± 10.4 kPa 20% strain: 135 kPa 40% strain: 600 kPa
Tran et al[24]	Human, 5 (all males)	Microindentation	$E = \Delta\sigma/\Delta\varepsilon$	Rest: 126 616 ± 76 349 dynes/cm^2 Low stimulation: 191 688 ± 111 854 dynes/cm^2 High stimulation: 215 894 ± 11 432 dynes/cm^2
Berke and Smith[23]	Canine, 5	Microindentation	$\varepsilon = \Delta X/X$; $\sigma = \Delta F/A$; $E = \sigma/\varepsilon$	Subject 1: 25% strain: 2.38e4 dynes/cm^2, 50% strain: 5.84e4 dynes/cm^2, 75% strain: 1.45e5 dynes/cm^2 Subject 2: 25% strain: 1.33e5 dynes/cm^2, 50% strain: 1.96e5 dynes/cm^2, 75% strain: 1.75e6 dynes/cm^2 Subject 3: 50% strain: 1e5 dynes/cm^2
Alipour and Titze[30]	Canine, 10	Longitudinal elongation	$\varepsilon = (L - L_0)/L_0$; $\sigma = A(e^{B\varepsilon} - 1)$; $E = \sigma/\varepsilon$	0–15% strain: 20.7 ± 2.4 kPa (body), 41.9 ± 7.1 kPa (cover)
Perlman and Durham[21]	Human	Longitudinal elongation		10% strain: 100 kPa
Perlman et al[35]	Canine, 7	Longitudinal elongation	$\sigma = FpL_0\,(1 + \varepsilon)/m$ $m = \rho A L_0(1 + \varepsilon)$ $E = F_p L_0(1/\varepsilon + 1)/m$	30% strain: 2.8e5 ± 9.27e4 dynes/cm^2 50% strain: 4.12e5 ± 1.51e5 dynes/cm^2
Ishizaka and Kaneko[36]	Human	Longitudinal elongation		$E_{const.} = 3.7$ kPa

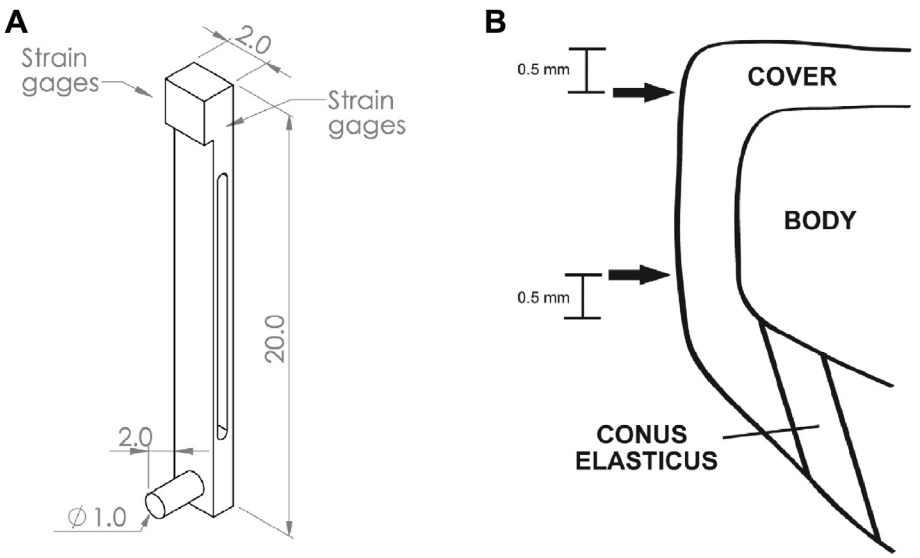

FIGURE 3. (**A**) Sketch detailing the customized load cell. All dimensions are in millimeters. (**B**) Schematic of a two-layer vocal fold model (coronal view). Loading and unloading measurements were taken at the superior and inferior aspects of the fold. The arrows indicate the location for the center of the probe tip.

to elicit phonation for a concurrent study examining intraglottal flow characteristics (Oren et al[14]). The stitch was tied with the minimal tension needed to have a prephonatory width of 0 mm between the vocal processes. Stress measurements were taken by gently retracting one fold using a vein retractor (Grieshaber, SS Cushing Design Vein Retractor 8-1/2; Alcon Surgical Inc, Fort Worth, TX) to allow insertion of the load cell.

The load cell was connected to a motorized traverse system (BiSlide and VXM motor; Velmex, Inc., Bloomfield, NY) and the tissue was indented in 0.1 mm increments at 0.5 Hz. A total of 1000 data points were recorded at a 1 kHz sampling rate for each station. The output signal from the load cell was captured using a National Instruments data acquisition system (PXIe-6356; National Instruments, Austin, TX). The mean voltage at each station was converted into a force value based on a known calibration. The action of the traverse was controlled in LabVIEW (National Instruments, Austin, TX). The maximum lateral displacement in each fold was determined based on the maximum glottal opening during phonation that was observed by high-speed imaging taken in the concurrent study. Loading and unloading testing in each larynx was repeated three times (starting at the same reference point at the superior edge), and the ensemble average of the stress-strain data was calculated from the measurements at each station. The mean maximum lateral displacement for all vocal folds was 1.5 mm (±0.3 mm).

The testing was performed by indenting the tissue at the mid-membranous plane, defined as the mid distance between the anterior commissure and the vocal process. At this location, the tissue was assumed to be incompressible (Berry and Titze[27] and Chan and Titze[28]). Measurements were taken at the superior and inferior aspects of the folds (Figure 3B). The displacement at the superior edge was made by vertically aligning the top of the probe tip with the superior edge of the fold using x3.5 surgical loupes (ie, the center of the probes tip was located 0.5 mm below the superior edge). After completion of superior indentation testing, the load cell was lowered so that the bottom of the probe tip was aligned with the inferior edge of the fold (ie, the center of the probe tip was located 0.5 mm above the inferior edge), and inferior aspect testing was performed. The vertical distance that the probe was lowered was based on the previously measured height of the vocal fold.

The stress in the tissue was calculated by dividing the force measurements by the contact area with the tissue, equivalent to the total area of the probe tip, $\sigma = F/A_{tip}$. The strain in the tissue was estimated using Green's strain, $\varepsilon_G = (L_0^2 - L^2)/2L_0^2$, where L_0 is the undeformed width of the tissue and L is the deformed width. The stiffness of the tissue was evaluated using the tangential Young's modulus, $E = d\sigma/d\varepsilon_G$. The slope for each measurement point was calculated using the central difference theorem (Fausett[29]).

Validation of the measurement technique was performed using a silicone model (Ecoflex 0010; Smooth-On Inc., Easton, PA) prepared according to the protocol of Chhetri et al.[22] The silicone sample was mounted on the testing apparatus and was indented 2 mm by the load cell using the same indentation testing protocol as described above.

RESULTS

The loading and unloading measurements obtained using the silicone model are shown in Figure 4. The tip of the probe was displaced approximately 0.5 mm before contact was made with the silicone material. The force measurements shown are comparable with the values measured by Chhetri et al.[22] Chhetri et al showed that the indentation depth should be equal to or less than to the indenter diameter, which stems from the fact that larger displacements (with respect to the tip diameter) may result in contact between parts of the probe other than the probe's tip and the testing material. If additional contact area is made with the testing material, it will directly affect

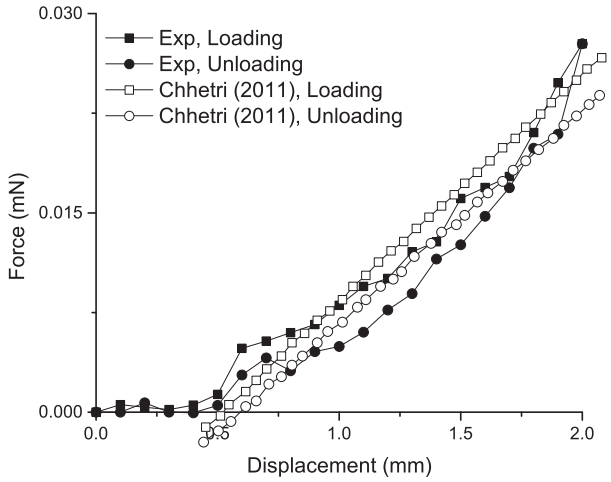

FIGURE 4. Loading and unloading curves for the silicone model. Current data are compared with the measurements of Chhetri et al.[22]

the accuracy of the force measurements (and consequently the stress calculations). Chhetri et al showed the loading and unloading data for a 5.5-mm tip diameter probe. Figure 4 demonstrates that the current 1-mm tip diameter probe can displace the soft silicone material more than 1.5 mm without contaminating the force measurements.

The stress-strain curves generated from larynx L1 are shown in Figure 5A. The curves represent an ensemble average from three experimental trials. Tissue hysteresis is observed in both aspects of the folds. The figure also shows that as the magnitude of the strain is increased, the stress in the inferior aspect increases more rapidly than the stress measured in the superior aspect. The hysteresis of the tissue and the increased stress in the inferior aspect were observed in all the other experimental cases (ie, larynges L2–L11).

The stress-strain data during unloading for all larynges is shown in Figure 5B. The solid lines represent the exponential fit to the stress-strain data based on the form: $\sigma = A(e^{B\varepsilon} - 1)$ (Alipour and Titze[30]). The shaded areas are the 95% confidence interval to the data fit. The figure shows that for low strain values, there is little difference in stress between the superior and inferior aspects of the folds. As the strain level is increased, the magnitude of the stress increases more in the inferior aspect compared with the superior aspect. Based on the curve fit to the data, at 40% strain, the mean stress in the inferior aspect is 13.6 kPa compared with 10 kPa at the superior aspect, which amounts to about 27% difference.

The local Young's modulus was calculated as the slope of the fit lines from the unloading stress-strain data (Figure 6). The unloading curve was used to determine the Young's modulus because it neglects measurement artifacts caused by global tissue displacement (Oliver and Pharr[31]). The nonlinearity of the stress-strain curves establishes that the stiffness of vocal fold tissue changes as a function of strain. Figure 6 shows that the stiffness of the inferior aspect is slightly higher (10%) than the superior aspect with no tissue strain. This difference is less than the 36% difference than that was measured by Chhetri et al[22] in a human larynx. As strain level increases, the inferior aspect becomes more differentially stiff than the superior. Based on the mean (ie, curve fit) data, at 40% strain, the inferior aspect is 35% stiffer than is superior aspect (48 kPa at the inferior aspect of the fold compared with 30 kPa at the superior aspect). Figure 6 shows that a global value for the Young's modulus does not exist; rather, the local stiffness of the tissue changes as a function of tissue strain.

DISCUSSION

The present study evaluated the elastic properties in the superior and inferior aspects of vocal folds at the mid-membranous plane. Testing of the vocal folds was done *in vitro* using an excised canine model. Results from 11 canine larynges show that the stiffness of the vocal fold tissue, which is measured by its differential Young's modulus, changes as a function of tissue strain. At low strain values, the magnitude

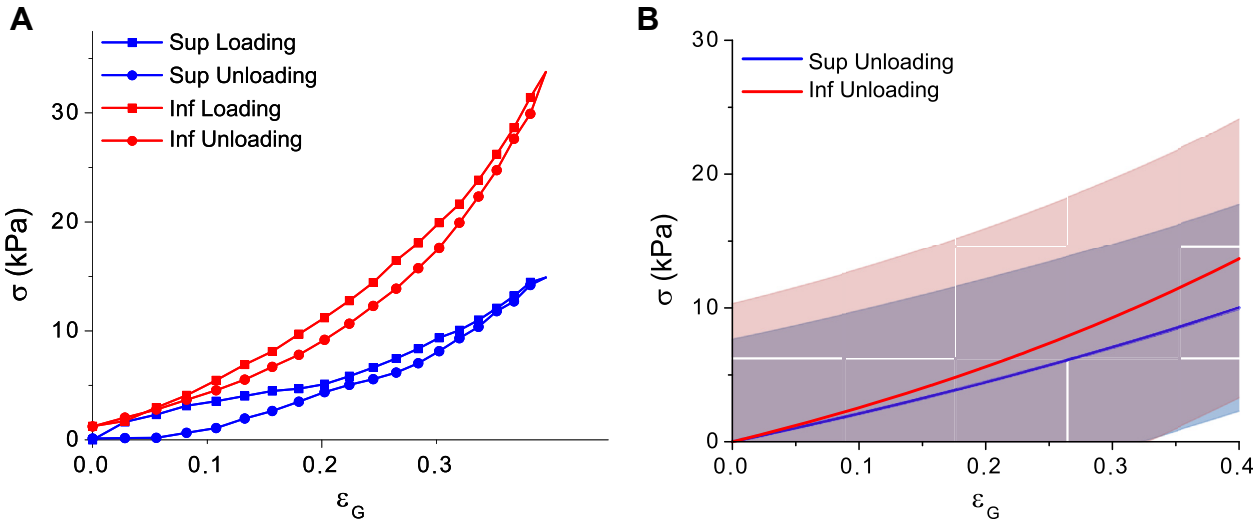

FIGURE 5. (**A**) Stress strain curve for the larynx L1 at the mid-membranous plane. The vertical height of the fold was 2.5 mm. Measurements are taken at 0.1 mm intervals. (**B**) Stress-strain data during unloading for larynges L1–L11. The solid lines are the exponential fit to the data. The shaded regions represent the 95% confidence interval.

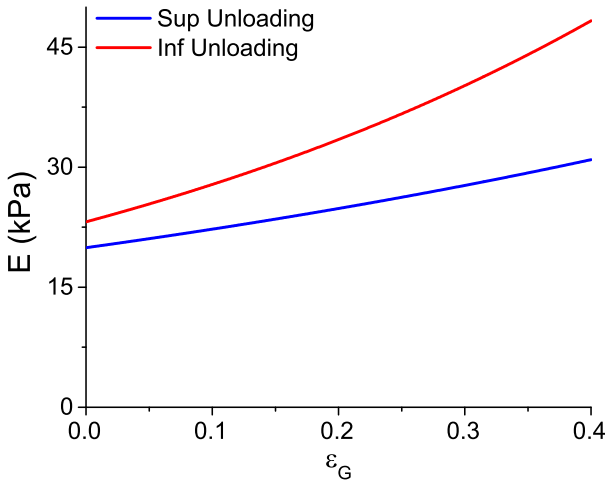

FIGURE 6. Young's modulus of the inferior and superior aspects of the vocal fold tissue as a function of strain. $E = d\sigma/d\varepsilon_G$. The modulus is calculated based on the curve fit line of the unloading data.

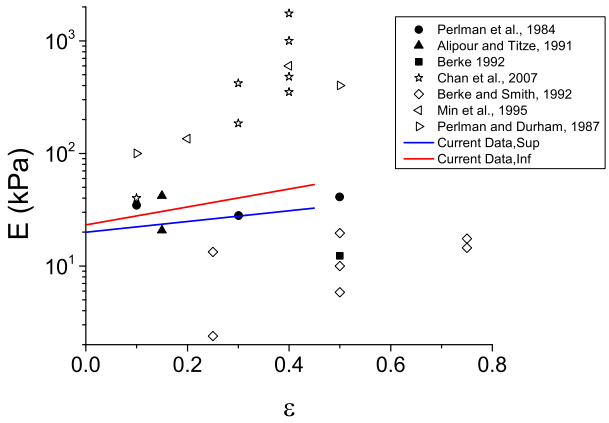

FIGURE 7. Reported values for the Young's modulus of the vocal folds in the literature. Closed symbols are from canine models. Open symbols are from human data. Current data are shown as solid lines.

of Young's modulus is similar in the inferior and superior aspects of the folds. As the magnitude of strain in the tissue is increased, which occurs due to larger lateral displacement of the folds, the stress increases exponentially and a stiffness gradient is formed along the glottal wall.

The increased stiffness observed at the inferior edge could be due to the proximity of the conus elasticus, a collagenous ligament that is continuous with the inferior edge (Figure 3B). TA muscle innervation would increase muscular tone in the glottis and could also increase measured stiffness of the tissue.

The interactions between the elastic properties of the vocal fold tissue and the aerodynamic forces from the glottal flow determine the characteristics of vocal fold vibration. Our current work shows that the glottal shape during closing (ie, the divergence angle) is dependent on the subglottal pressure. At low subglottal pressures (0–5 cmH_2O above phonation threshold), the divergence angle is minimal or does not exist. At these pressures, the airflow that passes through the glottis only imparts a small amount of lateral force on the vocal folds, which yields a small amount of lateral displacement (low strain values) and lower stress values. Consequently, the value of the Young's modulus is similar in both the superior and inferior aspects of the vocal fold. The lateral force that is applied by the glottal flow at both aspects will result in almost identical displacements, yielding no divergence angle. Conversely, at higher subglottal pressures (ie, 15–25 cmH_2O above phonation threshold), airflow passing through the glottis imparts a large amount of lateral force on the vocal folds. Similar to the preceding argument, at high strain values, the inferior aspect of the vocal fold is much stiffer than the superior edge; thus, any lateral force that is applied at both aspects will result in a much greater displacement of the superior edge, yielding a large divergence angle.

The current data show that the divergence angle is determined by a combination of factors. The current findings supplement the classical theory that shows a vertical phase delay of the mucosal wave. Other studies (Pickup and Thomson[32] and Smith and Thomson[33]) showed that the prephonatory glottal shape can also affect the divergence angle. Characterizing the superior-inferior difference in stiffness is needed to better characterize the recoil forces and tissue elasticity that are used to model the vibration mechanism of the folds. The current data also show that different values for stiffness are needed for the superior and inferior aspects of the folds and that these values change as a function of strain. The effect, if any, of an increased divergence angle during the closing phase on the acoustical intensity of the voice still needs to be determined.

A possible weakness of the present study is that adduction of the folds was made by suturing the vocal processes together in lieu of stimulation of the laryngeal muscles. Placing the suture in the vocal process created some prestress condition in the tissue that cannot be quantified. Additionally, it cannot be determined if the prestress magnitude is independent of the larynx being used. It is important to quantify the effect of using a suture to adduct the folds because it has been shown that different excitation levels of laryngeal muscle excitation (ie, different magnitudes of prestress) can change the dynamics and the acoustic characteristics of the folds (Chhetri et al[34]). The present study also did not account for the viscoelastic response of the vocal fold tissue, and the resultant measures of the Young's modulus of the tissue may be overestimated.

The model of Story and Titze[11] shows that the divergence angle depends on the stiffness of the body, which is raised by increasing the TA activation, and the stiffness of the cover layer, which is raised by increasing the cricothyroid (CT) activation. When both TA and CT activation are either small or large there is minimal divergence. The maximal divergence occurs when the TA is much more activated than the CT. These predicted results need experimental validation.

The biomechanical properties of the vocal folds are important characteristics needed to study the vibration mechanism of the folds. The previously reported literature data for these properties vary both quantitatively and qualitatively. These variations stem from the nonlinearity of the elastic properties of the tissue, the difference in the methodologies used to evaluate these properties (eg, the direction that the stress is applied and calculated), if part(s) of the tissue were removed, and how the Young's modulus was calculated. Additionally, it is

difficult to quantify the effect of tissue decay on the cellular integrity when using *ex vivo* models. Figure 7 summarizes the data from Table 1 and the data from the present study. The values for the Young's modulus are plotted on a logarithmic scale. The figure demonstrates that there is a large variation in the literature data and suggests that selection of the right value(s) for Young's modulus will depend on the model being used and what question the model is attempting to answer.

Acknowledgment

The authors acknowledge the support of National Institutes of Health grant no. 5R01DC009435.

REFERENCES

1. Hirano M. *Clinical Examination of Voice*. Wien, Austria: Springer-Verlag; 1981.
2. Jiang JJ, Titze IR. A methodological study of hemilaryngeal phonation. *Laryngoscope*. 1993;103:872–882.
3. Titze IR, Alipour F. *The Myoelastic Aerodynamic Theory of Phonation*. Iowa City, IA: National Center for Voice and Speech; 2006:1–61. Ch. 1.
4. Shadle CH, Barney A, Davies P. Fluid flow in a dynamic mechanical model of the vocal folds and tract. II. Implications for speech production studies. *J Acoust Soc Am*. 1999;105:456–466.
5. Pelorson X, Hirschberg A, Van Hassel R, Wijnands A, Auregan Y. Theoretical and experimental study of quasisteady-flow separation within the glottis during phonation. application to a modified two-mass model. *J Acoust Soc Am*. 1994;96:3416–3431.
6. Alipour F, Titze I. Combined simulation of two-dimensional airflow and vocal-fold vibration. *J Acoust Soc Am*. 1997;102:3204.
7. Zhao W, Zhang C, Frankel S, Mongeau L. Computational aeroacoustics of phonation, part I: computational methods and sound generation mechanisms. *J Acoust Soc Am*. 2002;112:2134–2146.
8. Kucinschi B, Scherer R, DeWitt K, Ng T. Flow visualization and acoustic consequences of the air moving through a static model of the human larynx. *J Biomech Eng*. 2006;128:380–390.
9. Anderson J. *Fundamentals of Aerodynamics*. New York, NY: McGraw-Hill; 2007:98–144. Ch. 2.
10. Ishizaka K, Flanagan JL. Synthesis of voiced sounds from a two-mass model of the vocal cords. *Bell Syst Tech J*. 1972;51:1233–1268.
11. Story B, Titze I. Voice simulation with a body-cover model of the vocal folds. *J Acoust Soc Am*. 1995;97:1249–1260.
12. Zhang C, Zhao W, Frankel S, Mongeau L. Computational aeroacoustics of phonation, part ii: effects of flow parameters and ventricular folds. *J Acoust Soc Am*. 2002;112:2147–2154.
13. Mihaescu M, Khosla S, Murugappan S, Gutmark E. Unsteady laryngeal airflow simulations of the intra-glottal vortical structures. *The J Acoust Soc Am*. 2010;127:435–444.
14. Oren L, Gutmark E, Khosla S. Intraglottal geometry and velocity measurements in canine larynges, *J Acoust Soc Am*. (in press).
15. Titze IR. The physics of small-amplitude oscillation of the vocal folds. *J Acoust Soc Am*. 1988;83:1536–1552.
16. Story BH. An overview of the physiology, physics and modeling of the sound source for vowels. *Acoust Sci Technol*. 2002;23:195–206.
17. Hirano M. Morphological structure of the vocal cord as a vibrator and its variations. *Folia Phoniatr*. 1974;26:89–94.
18. Titze IR. Physiologic and acoustic differences between male and female voices. *J Acoust Soc Am*. 1989;85:1699–1707.
19. Chan RW, Fu M, Young L, Tirunagari N. Relative contributions of collagen and elastin to elasticity of the vocal fold under tension. *Ann Biomed Eng*. 2007;35:1471–1483.
20. Min Y, Titze I, Alipour-Haghighi F. Stress-strain response of the human vocal ligament. *Ann Otol Rhinol Laryngol*. 1995;104:563–569.
21. Perlman A, Durham P. In vitro studies of vocal fold mucosa during isometric conditions. In: Baer T, Sasaki C, Harris K, eds. *Laryngeal Function in Phonation and Respiration*. Boston, MA: College-Hill Press; 1987: 291–303.
22. Chhetri DK, Zhang Z, Neubauer J. Measurement of young's modulus of vocal folds by indentation. *J Voice*. 2011;25:1–7.
23. Berke G, Smith M. Intraoperative measurement of the elastic modulus of the vocal fold. part 2. Preliminary results. *Laryngoscope*. 1992;102: 770–778.
24. Tran Q, Gerratt B, Berke G, Kreiman J. Measurement of young's modulus in the in vivo human vocal folds. *Ann Otol Rhinol Laryngol*. 1993;102: 584–591.
25. Goodyer E, Welham NV, Choi SH, Yamashita M, Dailey SH. The shear modulus of the human vocal fold in a transverse direction. *J Voice*. 2009; 23:151–155.
26. Fung YC. In: *Biomechanics: Motion, Flow, Stress, and Growth*, 1990;Vol 990. New York, NY: Springer-Verlag; 1990.
27. Berry DA, Titze IR. Normal modes in a continuum model of vocal fold tissues. *J Acoust Soc Am*. 1996;100:3345–3354.
28. Chan RW, Titze IR. Viscoelastic shear properties of human vocal fold mucosa: measurement methodology and empirical results. *J Acoust Soc Am*. 1999;106:2008–2021.
29. Fausett LV. *Applied Numerical Analysis Using Matlab*. Upper Saddle River, NJ: Prentice Hall; 1999:365–375. Ch. 11.
30. Alipour-Haghighi F, Titze IR. Elastic models of vocal fold tissues. *J Acoust Soc Am*. 1991;90:1326–1331.
31. Oliver WC, Pharr GM. Measurement of hardness and elastic modulus by instrumented indentation: advances in understanding and refinements to methodology. *J Mater Res*. 2004;19:3–20.
32. Pickup BA, Thomson SL. Identification of geometric parameters influencing the flow-induced vibration of a two-layer self-oscillating computational vocal fold model. *J Acoust Soc Am*. 2011;129:2121–2132.
33. Smith SL, Thomson SL. Influence of subglottic stenosis on the flow-induced vibration of a computational vocal fold model. *J Fluids Struct*. 2012;38:77–91.
34. Chhetri DK, Neubauer J, Bergeron JL, Sofer E, Peng KA, Jamal N. Effects of asymmetric superior laryngeal nerve stimulation on glottic posture, acoustics, vibration. *Laryngoscope*. 2013;123(12):3110–3116.
35. Perlman A, Titze I, Cooper D. Elasticity of canine vocal fold tissue. *J Speech Hear Res*. 1984;27:212.
36. Ishizaka K, Kaneko T. On equivalent mechanical constants of the vocal cords. *J Acoust Soc Jpn*. 1968;24:312–313.